The Astrophysical Journal Letters, 779:L23 (7pp), 2013 December 20 doi:10.1088/2041-8205/779/2/L23

NO TRANSIT TIMING VARIATIONS IN WASP-4

R. Petrucci[1,2,5], E. Jofré[2,3,5], M. Schwartz[1,2], V. Cúneo[2,3], C. Martínez[3], M. Gómez[2,3], A. P. Buccino[1,2,4], and P. J. D. Mauas[1,2]
[1] Instituto de Astronomía y Física del Espacio (IAFE), Buenos Aires, Argentina
[2] CONICET, Consejo Nacional de Investigaciones Científicas y Técnicas, Argentina
[3] Observatorio Astronómico de Córdoba, Córdoba, Argentina
[4] Departamento de Física, FCEN, Universidad de Buenos Aires, Buenos Aires, Argentina
Received 2013 October 4; accepted 2013 October 29; published 2013 December 4

ABSTRACT

We present six new transits of the system WASP-4. Together with 28 light curves published in the literature, we perform a homogeneous study of its parameters and search for variations in the transits' central times. The final values agree with those previously reported, except for a slightly lower inclination. We find no significant long-term variations in i or $R_P/R_\star$. The O–C mid-transit times do not show signs of transit timing variations greater than 54 s.

Key words: planetary systems – stars: individual (WASP-4) – techniques: photometric

Online-only material: color figures

1. INTRODUCTION

WASP-4b is one of the most studied exoplanets in the literature. Since its discovery (Wilson et al. 2008), many observations of this target have been made and several authors have determined the physical properties of the host-star and the exoplanet (Gillon et al. 2009; Winn et al. 2009; Nikolov et al. 2012). These works reveal that the system is formed by a G7V star with a close-in hot Jupiter ($M_p = 1.28\,M_J$, $R_p = 1.39\,R_J$) in a circular orbit which transits the star every 1.33 days. WASP-4b is a highly irradiated planet with a radius larger than that predicted by models (Fortney et al. 2007). One possibility is that ongoing orbital circularization provides the heat needed to inflate the planet (Beerer et al. 2011).

The transit timing variation (TTV) technique has proven to be a very promising method for estimating the mass of a non-transiting planet when it is not possible to obtain radial velocity measurements (Holman & Murray 2005). Since the time between transits of a single planet should be constant, variations in this time can be due to gravitational interaction with another planet in the system. If both planets show transits, it is possible to estimate the radius and mass for each of them, even without spectroscopic observations. Thus, it is possible to determine the densities of planets orbiting late stars. This is one of the key aspects of the TTV technique.

Different authors have unsuccessfully carried out TTVs analysis in the search for another planetary-mass body in the WASP-4 system. However, most of them employed mid-transit times fitted with different models and error treatments. As has been shown (Southworth et al. 2012; Nascimbeni et al. 2013), a lack of homogeneity in analysis techniques can lead to incorrect conclusions regarding TTVs.

In this work we present the light curves of six new transits of WASP-4b obtained with two telescopes located in Argentina, and perform a homogeneous study of TTVs, analyzing 34 light curves spanning 6 yr of observations. We employed the same fitting procedure and error treatment for all of these transits to obtain consistent photometric and physical parameters for the star and the exoplanet.

In Section 2 we present our observations and data reduction; in Section 3 we describe the procedure used to fit the light curves and the parameters derived for the 34 transits. In Section 4 we discuss the newly calculated ephemeris. In Section 5 we compare the results obtained with the fit provided by the Exoplanet Transit Database (ETD) and, finally, in Section 6 we present the conclusions.

2. OBSERVATIONS AND DATA REDUCTION

We observed six transits of WASP-4b between 2011 October and 2013 July, employing two different telescopes: the Horacio Ghielmetti Telescope (THG) located at the Complejo Astronómico El Leoncito (San Juan, Argentina), and the 1.54 m telescope located at the Estación Astrofísica de Bosque Alegre (EABA; Córdoba, Argentina). One of these transits was observed with both telescopes simultaneously. In the analysis, we considered these two measurements to be independent. In Table 1 we show a log of the observations.

The THG is a remotely operated 40 cm MEADE–RCX 400, with a focal ratio of $f/8$. The instrument is currently equipped with an Apogee Alta U16M camera with 4098 × 4098, 9 μm pixel, resulting in a scale of $0\farcs57$ pixel^{-1} and a $49' \times 49'$ field of view. At the EABA, we used the 1.54 m telescope in Newtonian focus, equipped with a 3070 × 2048, 9 μm pixel Apogee Alta U9 camera. This camera provides a scale of $0\farcs25$ pixel^{-1} and a $8' \times 12'$ field of view. For four transits, we employed the Johnson R filter available at both sites, while for the remaining two transits we made the observations without a filter.

At the beginning of each observing night, the computer clock was automatically synchronized with GPS. The central times of the images were expressed in a Heliocentric Julian Date based on Coordinated Universal Time ($HJD_{\rm UTC}$). Whenever possible, we observed for 90 minutes before and after each transit to obtain a large number of out-of-transit (OOT) data-points to correct possible trends in the light curves. We took ten bias frames, eight dark frames and between 15 and 20 dome flat-fields. We averaged all the biases and median-combined the bias-corrected darks. Finally, the bias- and dark-corrected flats were median-combined to generate a master flat in the corresponding

[5] Visiting Astronomer, Complejo Astronómico El Leoncito operated under agreement between the Consejo Nacional de Investigaciones Científicas y Técnicas de la República Argentina and the National Universities of La Plata, Córdoba and San Juan.

Table 1
Log of Our Observations

Date	Telescope	Camera	Filter	Bin-size	Exposure-time (s)	N_{obs}[a]	σ[b] (mag)
2011 Oct 17	THG	U16M	No filter	1 × 1	25	315	0.0059
2012 Aug 9	EABA	U9	No filter	1 × 1	40-50	306	0.0069
2012 Oct 11	EABA	U9	*R*	2 × 2	25	272	0.0019
2013 Jun 2	THG	U16M	R	2 × 2	180	68	0.0090
2013 Jun 6	THG	U16M	*R*	2 × 2	45	90	0.0063
2013 Jun 6	EABA	U9	*R*	2 × 2	90	141	0.0035

Notes.
[a] Number of data points.
[b] Standard deviation of the out-of-transit data points.

band. All of the images were processed using standard IRAF[6] tasks.

To obtain instrumental magnitudes with aperture photometry, we developed an algorithm called FOTOMCC. This is a quasi-automatic pipeline developed for the IRAF environment using the DAOPHOT package. Initially, FOTOMCC employs a reference image, previously selected by the user, to identify the centroids of the stars in all of the images. The optimal size for the aperture is chosen through the growth-curves technique (Howell 1989). Specifically, we adopted the aperture size for which the star magnitude was stable at the level of 0.001 mag. The width of the sky-subtraction annulus was set to 5 pixels. The magnitude errors were those provided by the DAOPHOT task.

To carry out differential photometry, we first subtracted the magnitude of each star in the field from the magnitude of the science star for every image. Then, we computed the standard deviation of all of the magnitude differences obtained in this way and selected those stars which produced light curves with a lower sigma value. Using the selected stars, we built a master star, the magnitude and error of which were the average magnitude and error of all of the chosen stars. The final light curve was built by subtraction of the magnitudes of the target and the master star. For each photometric data point, we estimated the formal error as the quadrature sum of the errors of the target star and the master star.

The light curves present smooth trends, mainly originating from differential extinction and/or spectral type differences between the comparison and the target star. To eliminate these slow variations, we fitted a Legendre polynomial to the OOT data-points and modified its order until the dispersion of the residuals was minimal. In almost all of the cases we used a second-order fit, although in some cases a lower dispersion was found by fitting a straight line. Finally, we removed the fit from all of the data for each light curve (including transit points) and normalized the OOT to unity. In Figure 1 we present our six light curves, and the best-fit to the data. Errorbars are also shown.

2.1. Archival Light Curves

To study TTVs and to determine the parameters, we also included all other publicly available transits. We considered, in particular, 20 light curves found in the literature: one from Wilson et al. (2008), two from Winn et al. (2009), one from Gillon et al. (2009), four from Sanchis-Ojeda et al. (2011) and twelve observed by Nikolov et al. (2012). We did not include the four transits from Southworth et al. (2009), since the authors reported failures in the computer clock which render the mid-transit times unreliable (Southworth et al. 2013). We also included eight transits observed by amateurs and published in the ETD[7]. We only analyzed complete transits with all four contact points clearly visible.

3. LIGHT-CURVE FITTING PROCEDURE

3.1. Photometric Parameters

Based on the HARPS high signal-to-noise archival spectra of WASP-4, we derived the following stellar parameters: effective temperature $T_{\rm eff}$, surface gravity $\log g$, metallicity [Fe/H], and microturbulence ξ, using the FUNDPAR code (Saffe 2011). The parameters obtained from the analysis are: $T_{\rm eff} = (5436 \pm 34)$ K, $\log g = (4.28 \pm 0.06)$ cm s^{-1}, $\xi = (0.94 \pm 0.03)$ km s^{-1}, and [Fe/H] $= (-0.05 \pm 0.04)$ dex (E. Jofré et al., in preparation). These agree with previously reported values, except for $\log g$ which is slightly lower (e.g., Doyle et al. 2013).

These stellar parameters were adopted as the initial input for the program JKTLD,[8] which calculates theoretical limb-darkening coefficients by bilinear interpolation of the effective temperature and surface gravity using different tabulations. In particular, we employed the tabulations provided by Van Hamme (1993) and Claret (2004). For those transits observed with no filter, we used bolometric limb-darkening coefficients.

All of the light curves were fitted using the JKTEBOP code.[9] This code models the light curve of a system of two components by performing numerical integration over the surface of concentric circles, under the assumption that the projection of each component is a biaxial ellipsoid. It employs the Levenberg–Marquardt optimization algorithm to obtain the best-fitting model. One of the advantages of JKTEBOP over other fitting models is that it considers small distortions from sphericity. Since WASP-4b is a bloated planet, this program can provide more realistic parameters from the observed data.

For each transit, we ran JKTEBOP following the same fitting procedure:

1. As free parameters we assumed: the inclination of the orbit (i); the sum of the fractional radii[10] ($r_\star + r_P$); the ratio

[6] IRAF is distributed by the National Optical Astronomy Observatories, which are operated by the Association of Universities for Research in Astronomy, Inc., under cooperative agreement with the National Science Foundation.

[7] http://var2.astro.cz/ETD.
[8] http://www.astro.keele.ac.uk/~jkt/codes/jktld.html.
[9] http://www.astro.keele.ac.uk/~jkt/codes/jktebop.html.
[10] $r_\star = R_\star/a$ and $r_P = R_P/a$ are the ratios of the absolute radii (of the star and the exoplanet respectively) to the semimajor axis.

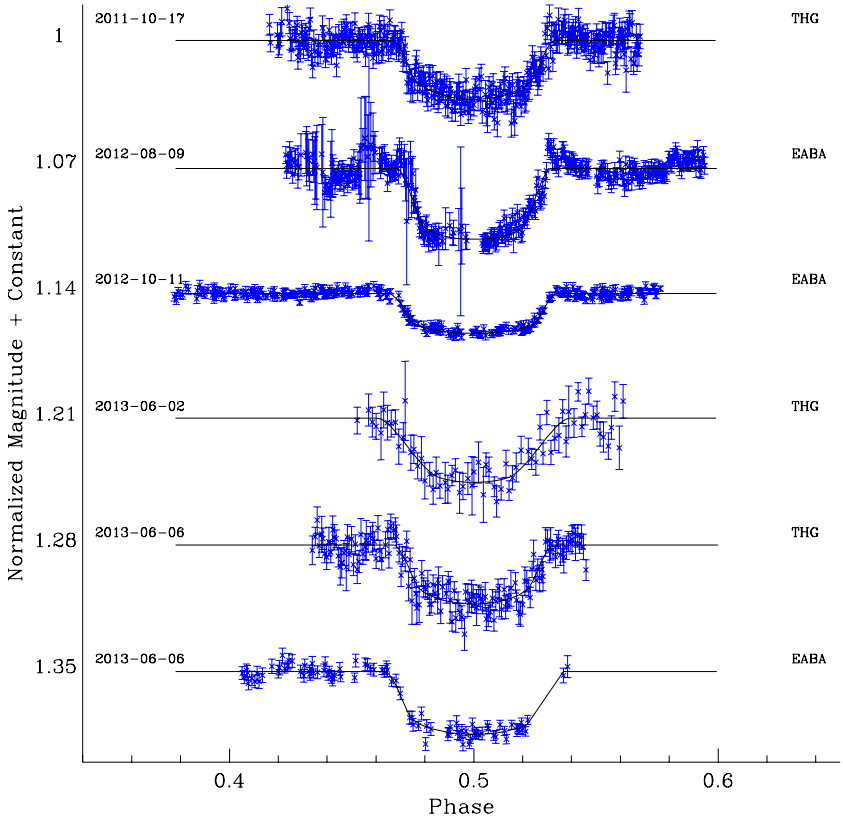

Figure 1. Light-curves presented in this work. The photometric observations and their error-bars are in blue. Black solid lines represent the best-fit to the data. For each transit, the date and the telescope are indicated.

(A color version of this figure is available in the online journal.)

of the fractional radii ($k = r_\star/r_P$); and the mid-transit time (T_0). We fitted every light curve with linear, quadratic, logarithmic, and square-root limb-darkening laws. For each case, we tried the analysis with (1) both coefficients fixed, (2) the linear coefficient fitted and the nonlinear fixed, and (3) both coefficients fitted. Finally, we adopted the model which minimized the χ^2 of the fit and provided realistic parameters as the best model for a given transit.

2. For a few transits, the convergence of some of the adjusted parameters was not achieved in 1. In these cases, assuming the limb-darkening law obtained in the first step, we iterated JKTEBOP, taking as the initial parameters for each iteration those obtained in the previous one. This process was repeated until convergence was obtained.
3. For the solution achieved in 2, we first multiplied the photometric errors by the square-root of the reduced chi-squared of the fit to get $\chi^2_r = 1$. Then, we ran the three algorithms available in JKTEBOP: Bootstrapping, Monte Carlo simulations, and Residual Permutation (RP), which takes red noise into account. For the first two options we performed 1000 iterations. We conservatively adopted the largest values given by these algorithms as the final errors of the parameters.

We adopted the median value of those obtained for every transit as the final value for every parameter (except for T_0, see Section 4). We adopted the asymmetric uncertainties σ_+ and σ_- of the selected distribution as the final error, since they are based on empirical data and are more realistic than those derived from a Gaussian distribution of the parameters.

3.2. Physical Parameters

The physical parameters were determined using standard formulae (Southworth 2009) implemented in the JKTABSDIM code.[11] This code requires as input the measured quantities: i, $r_\star$, r_P, the orbital period P, the velocity amplitudes of the star and the exoplanet, $K_\star$ and K_P respectively, the eccentricity e, $T_{\rm eff}$, [Fe/H], and their errors. For each light curve, we employed the photometric parameters (i, $r_\star$, r_P)[12] obtained with the program JKTEBOP, P determined from the ephemeris, and $T_{\rm eff}$ and [Fe/H] derived using HARPS spectra. We used $e = 0$, and the $K_\star$ value given by Triaud et al. (2010). The procedure was as follows. First, assuming $K_P = 150\,{\rm km\,s^{-1}}$, we calculated a stellar mass (see Equation (5) of Southworth 2009). By linearly interpolating this stellar mass and the [Fe/H] calculated in Section 3.1 within the tabulated theoretical model, we determined a predicted radius ($R_\star^{\rm (calc)}$) and effective temperature ($T_{\rm eff}^{\rm (calc)}$) for the star. Then, we evaluated the figure of merit:

$$\mathrm{fom} = \left[\frac{r_\star^{\rm (obs)} - (R_\star^{\rm (calc)}/a)}{\sigma(r_\star^{\rm (obs)})}\right]^2 + \left[\frac{T_{\rm eff}^{\rm (obs)} - T_{\rm eff}^{\rm (calc)}}{\sigma(T_{\rm eff}^{\rm (obs)})}\right]^2. \quad (1)$$

We repeated this process until we found the value for K_P which minimized Equation (1). In order to avoid any dependence on the stellar model, we performed this analysis for four different sets of stellar models: Y^2 (Demarque et al. 2004), Padova (Girardi et al. 2000), Teramo (Pietrinferni et al. 2004) and

[11] http://www.astro.keele.ac.uk/~jkt/codes/jktabsdim.html.

[12] The error considered as input was the larger between σ_+ and σ_-.

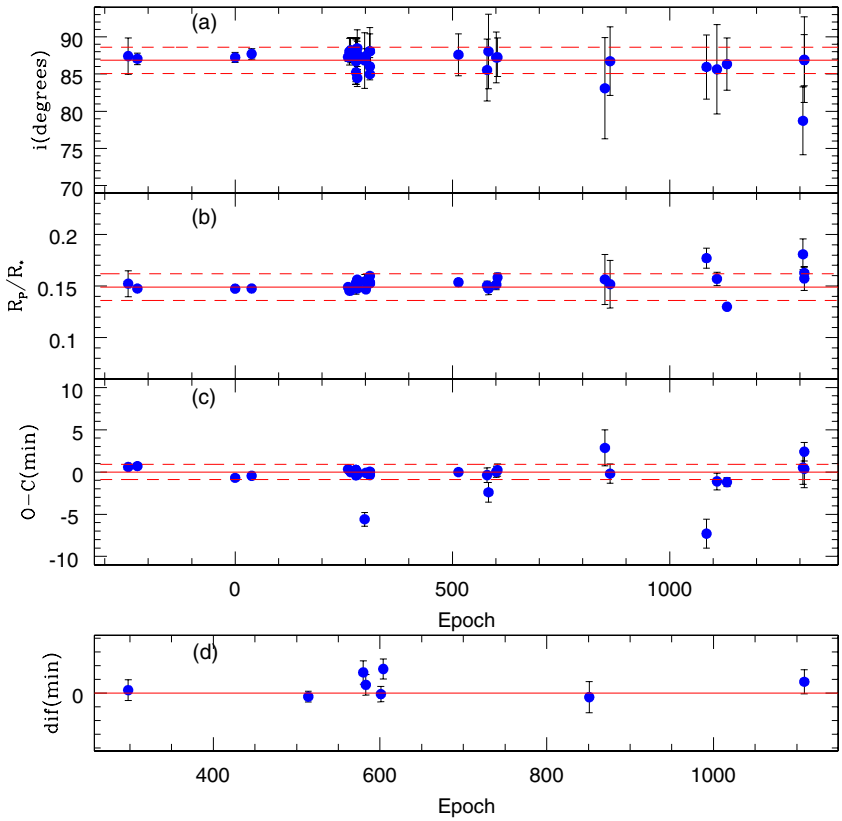

Figure 2. (a)–(c) i, $R_P/R_\star$ and O–C as a function of the transit epoch. Blue points are the values obtained for the 34 light curves. The solid and dashed horizontal red lines represent the weighted average and its $\pm 1\sigma$ errors, respectively. (d) Differences between the central transit times obtained with the model used in the ETD and those obtained in this work.

(A color version of this figure is available in the online journal.)

VRSS (VandenBerg et al. 2006). We adopted the average of the amplitudes given by each model as the final value for K_P, and the standard deviation as the error of the velocity. Finally, the solution for the system was determined using the JKTABSDIM code. From this procedure, we also estimated the age of the system considering series of models bracketing the lifetime of the star in the main sequence.

The resulting physical parameters of the star and the planet obtained for each transit are listed in Table 2. For the exoplanet, the surface gravity was calculated with:

$$g_P = \frac{2\pi}{P}\frac{\sqrt{(1-e^2)}K_\star}{r_P^2 \sin(i)} \quad (2)$$

(Southworth et al. 2007) and the modified equilibrium temperature as:

$$T'_{\rm eq} = T_{\rm eff}\sqrt{\frac{R_\star}{2a}} \quad (3)$$

(Southworth 2010). Therefore, both g_P and $T'_{\rm eq}$ are independent of the stellar models. We performed a weighted average of all the measurements to obtain the final value for each parameter, and the uncertainty was determined as the standard deviation of the sample. Table 3 shows the final values and errors calculated for the photometric and physical parameters of the star and the exoplanet. All of these are in good agreement with previous determinations, except for a slightly lower inclination.

The presence of a perturber in the system could produce long-term variations in these parameters (Sartoretti & Schneider 1999, Carter & Winn 2010). Considering that our data comprises 6 yr of observations, we studied the long-term behavior of i and $R_P/R_\star$ (Figures 2(a) and (b)). We found that these parameters remain constant within the $\pm 1\sigma$ error of the weighted average, except for the outlier data point in i corresponding to the epoch 1307, which could have been caused by variable observing conditions such as the presence of cirrus clouds during the observation night.

4. TRANSIT EPHEMERIS AND TIMING

We transformed the central times of all of the observations to a Barycentric Julian Date based on Barycentric Dynamical Time ($\rm BJD_{TDB}$) with the Eastman et al. (2010) online converter. For the amateur light curves, we contacted the observers when extra information was needed. For the mid-transit times we adopted the mean values obtained in Section 3, and considered the symmetric errors ($\pm\sigma$) given by the algorithm with the largest uncertainty. In most cases, the error obtained with the RP method was the largest, indicating the presence of red noise in the data (Pont et al. 2006). This implies that there are correlations between adjacent data points in a light curve, reducing the number of free parameters. The existence of red noise leads to an underestimation of the errors in the adjusted parameters which, in turn, might cause an inaccurate determination of the central time of the transit. The red noise can be quantified with the factor $\beta = \sigma_r/\sigma_N$, defined by Winn et al. (2008). Here, σ_r is obtained by averaging the residuals into M bins of N points and calculating the standard deviation of the binned residuals,

Table 2
Physical Properties of the Star and the Exoplanet Derived in This Work for the 34 Light Curves

Epoch	Date	i (°)	M_P ($M_{\rm Jup}$)	R_P ($R_{\rm Jup}$)	g_P (m s^{-2})	$T'_{\rm eq}$ (K)	$M_\star$ ($M_\odot$)	$R_\star$ ($R_\odot$)	$\log g_\star$ (cm s^{-1})	Age (Gyr)	a (AU)	Reference
−246	2007 Sep 25	87.42 ± 2.46	1.22 ± 0.032	1.349 ± 0.088	16.6 ± 2.8	1657 ± 56.5	0.894 ± 0.031	0.915 ± 0.052	4.467 ± 0.048	5.1 ± 3	0.02289 ± 0.00026	1
−225	2007 Oct 7	87.05 ± 0.76	1.218 ± 0.03	1.31 ± 0.028	17.5 ± 1.4	1657 ± 22.5	0.891 ± 0.029	0.914 ± 0.015	4.466 ± 0.012	5.5 ± 3	0.02287 ± 0.00025	2
0	2008 Aug 19	87.23 ± 0.68	1.215 ± 0.031	1.323 ± 0.028	17.2 ± 1.4	1666 ± 23.5	0.888 ± 0.03	0.923 ± 0.015	4.456 ± 0.012	6.8 ± 3	0.02284 ± 0.00026	3
38	2008 Oct 9	87.72 ± 0.72	1.226 ± 0.034	1.314 ± 0.025	17.5 ± 1.3	1654 ± 22.9	0.9 ± 0.033	0.914 ± 0.014	4.471 ± 0.01	5.1 ± 3.1	0.02294 ± 0.00028	3
260	2009 Aug 2	87.29 ± 0.59	1.217 ± 0.028	1.329 ± 0.023	17 ± 1.2	1660 ± 19	0.891 ± 0.026	0.918 ± 0.012	4.462 ± 0.009	5.7 ± 2.7	0.02286 ± 0.00022	4
263	2009 Aug 6	88.03 ± 1.80	1.218 ± 0.03	1.291 ± 0.027	18.1 ± 1.4	1656 ± 21.1	0.892 ± 0.028	0.914 ± 0.014	4.467 ± 0.01	5.3 ± 2.8	0.02287 ± 0.00024	4
266	2009 Aug 10	88.21 ± 1.70	1.217 ± 0.031	1.291 ± 0.037	18.1 ± 1.7	1656 ± 24.4	0.891 ± 0.03	0.913 ± 0.016	4.467 ± 0.013	5.4 ± 3	0.02286 ± 0.00026	4
278	2009 Aug 26	86.72 ± 3.07	1.206 ± 0.035	1.355 ± 0.111	16.2 ± 3.3	1680 ± 52.8	0.877 ± 0.032	0.934 ± 0.047	4.44 ± 0.043	8.8 ± 2.5	0.02274 ± 0.00028	5
278	2009 Aug 26	87.63 ± 2.23	1.219 ± 0.031	1.325 ± 0.083	17.2 ± 2.8	1664 ± 43.5	0.893 ± 0.03	0.922 ± 0.038	4.46 ± 0.035	5.9 ± 2.6	0.02288 ± 0.00026	5
278	2009 Aug 26	85.23 ± 1.60	1.195 ± 0.035	1.447 ± 0.087	14.1 ± 2.3	1717 ± 51	0.863 ± 0.033	0.971 ± 0.045	4.399 ± 0.039	11.2 ± 3.3	0.02262 ± 0.00029	5
278	2009 Aug 26	86.81 ± 2.81	1.208 ± 0.03	1.375 ± 0.068	15.8 ± 2.1	1677 ± 41.8	0.879 ± 0.028	0.932 ± 0.037	4.443 ± 0.033	8.5 ± 2	0.02276 ± 0.00024	5
281	2009 Aug 30	88.49 ± 2.47	1.231 ± 0.035	1.307 ± 0.107	17.8 ± 3.6	1654 ± 54.6	0.906 ± 0.033	0.916 ± 0.049	4.471 ± 0.046	4.1 ± 3	0.02299 ± 0.00028	5
281	2009 Aug 30	84.47 ± 1.15	1.195 ± 0.038	1.461 ± 0.069	13.8 ± 1.9	1711 ± 48	0.862 ± 0.037	0.964 ± 0.04	4.406 ± 0.035	11.3 ± 3.7	0.02261 ± 0.00032	5
281	2009 Aug 30	87.70 ± 2.14	1.223 ± 0.037	1.332 ± 0.093	17 ± 3.1	1655 ± 60.1	0.897 ± 0.036	0.913 ± 0.054	4.47 ± 0.051	4.6 ± 3.4	0.02291 ± 0.00031	5
281	2009 Aug 30	86.89 ± 2.53	1.217 ± 0.036	1.367 ± 0.069	16.1 ± 2.3	1666 ± 43.4	0.89 ± 0.034	0.923 ± 0.036	4.457 ± 0.033	6.8 ± 3.1	0.02285 ± 0.00029	5
298	2009 Sep 21	86.83 ± 3.75	1.206 ± 0.035	1.402 ± 0.248	15.1 ± 6	1687 ± 136	0.877 ± 0.032	0.942 ± 0.14	4.433 ± 0.13	8.8 ± 2.6	0.02274 ± 0.00028	6
301	2009 Sep 26	87.42 ± 1.00	1.218 ± 0.03	1.31 ± 0.032	17.5 ± 1.5	1661 ± 25.9	0.892 ± 0.029	0.919 ± 0.019	4.462 ± 0.016	6.2 ± 2.6	0.02287 ± 0.00025	4
310	2009 Oct 8	88.06 ± 2.34	1.234 ± 0.031	1.347 ± 0.107	16.8 ± 3.3	1643 ± 52.8	0.909 ± 0.029	0.904 ± 0.048	4.484 ± 0.046	3.7 ± 2.4	0.02302 ± 0.00025	5
310	2009 Oct 8	84.99 ± 0.78	1.202 ± 0.03	1.484 ± 0.05	13.5 ± 1.4	1699 ± 37.8	0.869 ± 0.029	0.953 ± 0.032	4.419 ± 0.028	10.1 ± 2.6	0.02268 ± 0.00025	5
310	2009 Oct 8	86.02 ± 1.22	1.213 ± 0.029	1.382 ± 0.068	15.7 ± 2.1	1673 ± 44.5	0.884 ± 0.027	0.929 ± 0.04	4.448 ± 0.037	7.4 ± 2.3	0.0228 ± 0.00023	5
310	2009 Oct 8	88.09 ± 3.16	1.234 ± 0.031	1.333 ± 0.14	17.2 ± 4.2	1641 ± 74.2	0.909 ± 0.029	0.903 ± 0.072	4.486 ± 0.069	3.7 ± 2.3	0.02302 ± 0.00025	5
514	2010 Jul 7	87.60 ± 2.83	1.226 ± 0.037	1.362 ± 0.159	16.3 ± 4.5	1653 ± 84.3	0.9 ± 0.036	0.912 ± 0.081	4.472 ± 0.077	4.5 ± 3.5	0.02294 ± 0.00031	7
580	2010 Oct 4	85.55 ± 4.17	1.212 ± 0.036	1.353 ± 0.201	16.4 ± 5.5	1669 ± 95.8	0.882 ± 0.031	0.924 ± 0.095	4.452 ± 0.089	7.7 ± 2	0.02279 ± 0.00027	8
583	2010 Oct 7	88.05 ± 5.01	1.232 ± 0.035	1.293 ± 0.299	18.2 ± 9.1	1644 ± 153.8	0.907 ± 0.033	0.905 ± 0.158	4.482 ± 0.153	4 ± 2.9	0.023 ± 0.00028	8
601	2010 Nov 1	87.24 ± 3.42	1.231 ± 0.031	1.336 ± 0.202	17 ± 5.8	1651 ± 143.6	0.905 ± 0.029	0.912 ± 0.149	4.475 ± 0.143	3.6 ± 2.3	0.02298 ± 0.00024	9
604	2010 Nov 5	87.26 ± 2.60	1.233 ± 0.03	1.38 ± 0.155	16 ± 4.2	1634 ± 83.6	0.908 ± 0.028	0.895 ± 0.082	4.493 ± 0.08	3.6 ± 2.3	0.023 ± 0.00024	8
851	2011 Oct 1	83.10 ± 6.80	1.188 ± 0.06	1.553 ± 0.796	12.2 ± 13.2	1779 ± 265.8	0.85 ± 0.045	1.037 ± 0.292	4.336 ± 0.251	14.6 ± 1.6	0.02251 ± 0.0004	6
863	2011 Oct 17	86.74 ± 4.62	1.223 ± 0.029	1.355 ± 0.235	16.5 ± 6.3	1672 ± 171.4	0.895 ± 0.026	0.932 ± 0.182	4.451 ± 0.172	5.2 ± 1.7	0.0229 ± 0.00022	10
1085	2012 Aug 9	85.95 ± 4.30	1.235 ± 0.036	1.51 ± 0.256	13.4 ± 5.1	1628 ± 156.1	0.908 ± 0.031	0.888 ± 0.16	4.499 ± 0.158	3.6 ± 2.2	0.02301 ± 0.00026	11
1109	2012 Sep 10	85.64 ± 6.01	1.202 ± 0.045	1.457 ± 0.333	14 ± 7.1	1698 ± 213	0.871 ± 0.039	0.953 ± 0.225	4.42 ± 0.209	9.6 ± 3.1	0.02269 ± 0.00033	12
1132	2012 Oct 11	86.34 ± 3.50	1.204 ± 0.036	1.202 ± 0.101	20.6 ± 4.3	1693 ± 67.3	0.874 ± 0.034	0.949 ± 0.063	4.426 ± 0.057	9.2 ± 2.6	0.02272 ± 0.00029	11
1307	2013 Jun 2	78.72 ± 4.56	1.241 ± 0.111	2.252 ± 0.477	6 ± 3.2	1947 ± 222.6	0.892 ± 0.108	1.262 ± 0.238	4.186 ± 0.163	13 ± 6.3	0.02287 ± 0.00092	10
1310	2013 Jun 6	86.93 ± 5.76	1.22 ± 0.035	1.34 ± 0.359	16.8 ± 9.7	1661 ± 155.6	0.894 ± 0.029	0.92 ± 0.162	4.462 ± 0.155	5 ± 1.8	0.02289 ± 0.00025	10
1310	2013 Jun 6	86.89 ± 3.44	1.196 ± 0.032	1.53 ± 0.271	12.6 ± 5	1712 ± 126.3	0.867 ± 0.03	0.966 ± 0.132	4.406 ± 0.119	10.8 ± 2.4	0.02266 ± 0.00026	11

Notes. References: (1) Wilson et al. (2008); (2) Gillon et al. (2009); (3) Winn et al. (2009); (4) Sanchis-Ojeda et al. (2011); (5) Nikolov et al. (2012); (6) Tifner (ETD); (7) Sauer (ETD); (8) Curtis (ETD); (9) T. G. Tan (ETD); (10) This work (THG); (11) This work (EABA); (12) Evans (ETD).

Table 3
Final Parameters of the WASP-4 System Derived in This Work

Parameter	Value	Error
Period P (days)	1.33823251	0.00000031
Minimum reference Time T_0 (BJD_{TDB})	2454697.797973	0.000076
Inclination i (°)	86.85	1.76
Stellar radius $R_\star$ ($R_\odot$)	0.92	0.06
Stellar mass $M_\star$ ($M_\odot$)	0.89	0.01
Stellar gravity $\log g_\star$ (cm s^{-1})	4.461	0.054
Semimajor axis a (UA)	0.0228	0.00013
Age (Gyr)	7.0	2.9
Stellar effective temperature $T_{\rm eff}$ (K)	5436	34
Metallicity [Fe/H] (dex)	−0.05	0.04
Planet radius R_P ($R_{\rm Jup}$)	1.33	0.16
Planet mass M_P ($M_{\rm Jup}$)	1.216	0.013
Planet surface gravity g_P ($m\,s^{-2}$)	16.41	2.49
Planet equilibrium temperature $T'_{\rm eq}$ (K)	1664	54

and σ_N is the expected deviation, calculated by:

$$\sigma_N = \frac{\sigma_1}{\sqrt{N}}\sqrt{\frac{M}{M-1}}, \quad (4)$$

where σ_1 is the standard deviation of the unbinned residuals. Considering that the duration of the ingress/egress of the WASP-4b transits is about 20 minutes, we averaged the residuals in bins of between 10 and 30 minutes and calculated the parameter β for each case. Finally, we used the median value as the red noise factor corresponding to that light curve. In the absence of red noise, we expect $\beta = 1$. For these transits β ranges from 0.58 to 2.36.

The whole sample of mid-transit times presents two large outliers corresponding to the epochs 298 and 1085. The first transit was obtained from the ETD. In the latter case, we believe that there was a failure in the computer clock. We did not consider these points for further analysis. Therefore, we determined the ephemeris in three different ways: (1) considering all of the 32 remaining transits; (2) excluding the incomplete transit (indicated in Figure 1 as 2013 June 6 and observed at EABA); and (3) only considering those transits with $\beta \leqslant 1.6$ (30 points). In the three cases we fitted the data through weighted least-squares to obtain the best period and the minimum reference time. We re-scaled the uncertainties, multiplying them by $\sqrt{\chi^2_r}$. The final values and errors for P and T_0 obtained from the different sets are:

$$\begin{aligned}
(1)\ P &= 1.33823251(31)\,\text{days},\\
T_0 &= 2454697.797973(76)\,\text{BJD}_{\rm TDB}\\
(2)\ P &= 1.33823251(32)\,\text{days},\\
T_0 &= 2454697.797973(77)\,\text{BJD}_{\rm TDB}\\
(3)\ P &= 1.33823227(32)\,\text{days},\\
T_0 &= 2454697.797973(77)\,\text{BJD}_{\rm TDB}.
\end{aligned}$$

Since there are no differences in T_0, the inclusion of partial transits, or those obtained with large red noise, does not affect the calculation. We adopted the ephemeris given by the sample (1), including all the transits.

With the new ephemeris, we calculated the O–C mid-transit times, which are shown in Figure 2(c). Except for the outliers mentioned already, all differences are within the $\pm 1\sigma$ error. The rms of the data is 54 s. We ran a Lomb–Scargle periodogram (Horne & Baliunas 1986) on the data, excluding the two large outliers, and no significant peak was found.

5. COMPARISON BETWEEN JKTEBOP AND THE FITTING MODEL IN THE ETD

For the light curves taken from the ETD, we compared the mid-transit times obtained with JKTEBOP and those given by the ETD, which provides an automatic fit, modeling the photometric data with the function (Poddany et al. 2010):

$$\begin{aligned}
m(t_i) = A - 2.5\log F(z[t_i, t_0, D, b],\, p, c_1)\\
+ B(t_i - t_{\rm mean}) + C(t_i - t_{\rm mean})^2, \quad (5)
\end{aligned}$$

where $m(t_i)$ are the relative magnitudes taken at the times t_i, N is the number of data points, $t_{\rm mean} = t_i/N$ is the mean time of the observations, z is the projected relative separation of the planet from the star, p is the ratio of the planet to star radii, and $F(z, p, c_1)$ is the *occultsmall* routine of Mandel & Agol (2002), giving the relative flux of the star as the planet transits. This model assumes a linear limb-darkening law with the coefficient c_1 fixed at an arbitrary value of 0.5. The user has the possibility of fitting or maintaining the mid-transit time, the duration, and the depth parameters as fixed. The coefficients of Equation (5) are calculated using the Levenberg–Marquardt nonlinear least-squares algorithm from Press et al. (1993). The optimal parameters are determined by iterating the procedure until the difference between two successive values of $\Delta\chi^2$ is negligible.

We fitted the three parameters simultaneously and converted the resulting $HJD_{\rm UTC}$ mid-transit times to $BJD_{\rm TDB}$. In Figure 2(d), we show the differences between the central times determined in both ways. The errorbars are those derived using the ETD model. The differences are as large as 1.5 minutes. We believe these disagreements are due to the very simple limb-darkening law assumed in the ETD fit. In any case, these differences indicate the need to derive the mid-transit times with a homogeneous method, when searching for TTVs.

6. SUMMARY AND CONCLUSIONS

In this work we present six new observations of transits of WASP-4b, observed between 2011 and 2013. Using these observations together with another 28 transits previously reported (including eight observed by amateurs), we performed a homogeneous study of the system, taking into account the realistic possibility of distortions in its components. The physical parameters of the star and the exoplanet are consistent with previous determinations, except for the inclination, which is slightly lower, probably due to the fitting procedure.

In addition, we analyzed the long-term behavior of different parameters. Except for one outlier in i, and two for the O–C mid-transit times, all of these parameters remain stable within the $\pm 1\sigma$ error of the weighted averages. The rms of the mid-transit times is 54 s. Therefore, we confirm previous results, and found that the system does not show significant TTVs attributable to the presence of a perturber, a conclusion we expanded with two more years of observations, to a baseline of 6 yr. The lack of temporal variations in the rest of the parameters supports this conclusion.

Finally, we report differences as large as 1.5 minutes between the mid-transit times modeled by the fitting programs provided by the ETD and JKTEBOP. Therefore, we believe that the central times provided by the ETD should be used with caution in TTV studies.

We are grateful to Pablo Perna and the staff at CASLEO for technical support, and to CONICET for funding this research.

We thank the anonymous referee for useful comments, and Phil Evans, Ivan Curtis, and T. G. Tan for kindly providing us with information about their observations.

REFERENCES

Beerer, I. M., Knutson, H. A., Burrows, A., et al. 2011, ApJ, 727, 23
Carter, J. A., & Winn, J. N. 2010, ApJ, 716, 850
Claret, A. 2004, A&A, 428, 1001
Demarque, P., Woo, J. H., Kim, Y. C., & Yi, S. K. 2004, ApJS, 155, 667
Doyle, A. P., Smalley, B., Maxted, P. F. L., et al. 2013, MNRAS, 428, 3164
Eastman, J., Siverd, R., & Gaudi, B. S. 2010, PASP, 122, 935
Fortney, J. J., Marley, M. S., & Barnes, J. W. 2007, ApJ, 668, 1267
Gillon, M., Smalley, B., Hebb, L., et al. 2009, A&A, 496, 259
Girardi, L., Bressan, A., Bertelli, G., & Chiosi, C. 2000, A&AS, 141, 371
Holman, M. J., & Murray, 2005, Sci, 307, 1288
Horne, J. H., & Baliunas, S. L. 1986, ApJ, 302, 757
Howell, S. B. 1989, PASP, 101, 616
Mandel, K., & Agol, E. 2002, ApJ, 580, 171
Nascimbeni, V., Cunial, A., Murabito, S., et al. 2013, A&A, 549, 30
Nikolov, N., Henning, T., Koppenhoefer, J., et al. 2012, A&A, 539, A159
Pietrinferni, A., Cassisi, S., Salaris, M., & Castelli, F. 2004, ApJ, 612, 168
Poddany, S., Brat, L., & Pejcha, O. 2010, NewA, 15, 297
Pont, F., Zucker, S., & Queloz, D. 2006, MNRAS, 373, 231
Press, W. H., Teukolsky, S. A., Vetterling, W. T., et al. 1993, Obs, 113, 214
Saffe, C. 2011, RMxAA, 47, 3
Sanchis-Ojeda, R., Winn, J. N., Holman, M. J., et al. 2011, ApJ, 733, 127
Sartoretti, P., & Schneider, J. 1999, A&AS, 134, 553
Southworth, J. 2009, MNRAS, 394, 272
Southworth, J. 2010, MNRAS, 408, 1689
Southworth, J., Bruni, I., Mancini, L., & Gregorio, J. 2012, MNRAS, 420, 2580
Southworth, J., Hinse, T. C., Burgdorf, M. J., et al. 2009, MNRAS, 399, 287
Southworth, J., Mancini, L., Browne, P., et al. 2013, MNRAS, 434, 1300
Southworth, J., Wheatley, P. J., & Sams, G. 2007, MNRAS, 379, 11
Triaud, A. H. M. J., Collier Cameron, A., Queloz, D., et al. 2010, A&A, 524, 25
VandenBerg, D. A., Bergbusch, P. A., & Dowler, P. D. 2006, ApJS, 162, 375
Van Hamme, W. 1993, AJ, 106, 2096
Wilson, D. M., Gillon, M., Hellier, C., et al. 2008, ApJ, 675, 113
Winn, J. N., Holman, M. J., Carter, J. A., et al. 2009, AJ, 137, 3826
Winn, J. N., Holman, M. J., Torres, G., et al. 2008, ApJ, 683, 1076